

**Variational and parquet-diagram calculations for neutron matter. V. Triplet pairing**E. Krotscheck <sup>1,2</sup>, P. Papakonstantinou <sup>3</sup> and J. Wang <sup>1</sup><sup>1</sup>*Department of Physics, University at Buffalo, SUNY, Buffalo, New York 14260, USA*<sup>2</sup>*Institut für Theoretische Physik, Johannes Kepler Universität, A 4040 Linz, Austria*<sup>3</sup>*Rare Isotope Science Project, Institute for Basic Science, Daejeon 34000, Korea*

(Received 3 August 2023; revised 26 October 2023; accepted 22 November 2023; published 5 January 2024)

We apply a large-scale summation of Feynman diagrams, including the class of parquet-diagrams *plus* important contributions outside the parquet class, for calculating effective pairing interactions and subsequently the superfluid gap in  $P$ -wave pairing in neutron matter. We employ realistic nucleon-nucleon interactions of the  $v_8$  type and perform calculations up to a Fermi momentum of  $1.8 \text{ fm}^{-1}$ . We find that many-body correlations lead to a strong reduction of the spin-orbit interaction, and, therefore, to an almost complete suppression of the  $^3P_2$  and  $^3P_2$ - $^3F_2$  gaps. We also find pairing in  $^3P_0$  states; the strength of the pairing gap depends sensitively on the potential model employed. Our results for triplet pairing are relevant for assessing superfluidity in neutron star interiors, whose presence can affect the cooling of neutron stars.

DOI: [10.1103/PhysRevC.109.015803](https://doi.org/10.1103/PhysRevC.109.015803)**I. INTRODUCTION**

Pairing is manifest in the spectra of finite nuclei, as recognized long ago [1], and is predicted to develop at various densities in nucleonic matter found in compact stars [2–6]. The most basic type of calculations of pairing and superfluidity or superconductivity in nuclear matter rely on mean-field-like (or Hartree-Fock-like) implementations of Bardeen-Cooper-Schrieffer (BCS) theory. It was recognized long ago that the BCS equations can be solved not only for soft interactions but also for interactions with a repulsive hard core [7]. To what extent a mean-field theory captures the essential physics of the nucleonic system is an important question.

In the case of pure neutron matter, theoretical approaches generally agree that the value of the  $S$ -wave pairing gap value should reach a maximum of roughly 2 MeV (within about 1 MeV) at a Fermi momentum somewhat below  $1 \text{ fm}^{-1}$ , corresponding to subsaturation densities [5,6,8–17]. There still remain some quantitative discrepancies. This is not surprising given the extreme sensitivity of the pairing gap to the interaction and also in view of the different ways effects beyond mean-field theory are taken into account, if at all. Similar conclusions seem valid for  $\beta$ -equilibrated matter [18].

The situation in the case of triplet  $P$ -wave pairing in neutron matter is much more uncertain. It is not even clear whether a pairing gap develops in this channel. The question is of particular astrophysical significance since triplet pairing is expected to be most favored at densities found in the outer liquid core of neutron stars and its presence would affect the cooling curves of neutron stars, i.e., the evolution of surface temperature with time [3,6,19]. Clarifying the question of triplet pairing is necessary in order to make the most of modern observational capabilities.

Microscopic calculations employing realistic nuclear potentials generally predict, at the mean-field level, a

nonvanishing triplet pairing gap [11,12,16,20,21]. However, at the high densities involved, effects beyond mean-field approximations cannot be neglected. For example, it has been found that realistic nucleon effective masses [20] and short-range correlations [22,23] can reduce or eliminate the gap [11]. Three-nucleon interactions of the Urbana IX family can also lead to vanishing gaps [24,25]. The effect of three-nucleon interactions derived within chiral effective field theory ( $\chi$ EFT) has been studied, too, and was found to be regulator dependent but potentially significant in the triplet channel [11,16].

Studies of polarization and screening effects in the triplet channel have been scarce. The in-medium spin-orbit and tensor interaction components are especially important, but they are not well understood. Even working with bare nucleon-nucleon potentials, the results for the triplet channel depend on the interaction type (e.g., Argonne, Bonn,  $\chi$ EFT, etc.). A study of polarization contributions to the spin-dependent nuclear interaction in the medium has suggested a suppression of the  $^3P_2$  gap [26].

It is the purpose of this work to apply a comprehensive diagrammatic theory to the problem of triplet pairing in neutron matter. Our method is based on an evaluation of Feynman diagrams that include self-consistently ring and ladder diagrams, i.e., the parquet class, but also totally irreducible diagrams, dubbed “twisted chains,” which become important when the interactions between particles in spin-singlet and spin-triplet states are very different. The method has been developed and applications were presented in a series of previous papers [17,27–29]. In Ref. [17], it was applied to the pairing gap problem in the singlet channel, and the effect of the correlations was discussed. The method was generalized in Ref. [29] to spin-orbit forces. It was demonstrated that many-body correlations affect dramatically the in-medium spin-orbit component, which in turn affects the triplet pairing

gap. The above result forms the motivation for the present work.

This paper is organized as follows. The theoretical background and details of the formalism for  $v_8$  bare potentials are presented in Sec. II. Results are presented and discussed in Sec. III. We summarize our findings in Sec. IV. The appendices contain additional information and technical details as well as some results with bare interactions for comparison with earlier work.

## II. MICROSCOPIC THEORY

### A. Interactions: Semiempirical nucleon-nucleon forces in operator representation

Accurate representations of the nucleon-nucleon potentials [30–33] are constructed to fit the interactions in each partial wave to scattering data and deuteron binding energies. For the purpose of identifying specific physical effects and of high-level many-body calculations, an interaction given in the form of a sum of local functions times operators acting on the spin, isospin, and possibly the relative angular momentum variables of the individual particles is preferred [32,34,35], i.e.,

$$\hat{v}(i, j) = \sum_{\alpha=1}^n v_{\alpha}(r_{ij}) \hat{O}_{\alpha}(i, j), \quad (2.1)$$

where  $r_{ij} = |\mathbf{r}_i - \mathbf{r}_j|$  is the distance between particles  $i$  and  $j$ . According to the number of operators  $n$ , the potential model is referred to as a  $v_n$  model potential. Semirealistic models for nuclear matter keep at least the six to eight base operators

$$\begin{aligned} \hat{O}_1(i, j; \hat{\mathbf{r}}_{ij}) &\equiv \hat{O}_c = \mathbb{1}, \\ \hat{O}_3(i, j; \hat{\mathbf{r}}_{ij}) &\equiv \boldsymbol{\sigma}_i \cdot \boldsymbol{\sigma}_j, \\ \hat{O}_5(i, j; \hat{\mathbf{r}}_{ij}) &\equiv S_{ij}(\hat{\mathbf{r}}_{ij}) \\ &\equiv 3(\boldsymbol{\sigma}_i \cdot \hat{\mathbf{r}}_{ij})(\boldsymbol{\sigma}_j \cdot \hat{\mathbf{r}}_{ij}) - \boldsymbol{\sigma}_i \cdot \boldsymbol{\sigma}_j, \\ \hat{O}_7(i, j; \mathbf{r}_{ij}, \mathbf{p}_{ij}) &\equiv \mathbf{r}_{ij} \times \mathbf{p}_{ij} \cdot \mathbf{S}, \\ \hat{O}_{2\alpha}(i, j; \hat{\mathbf{r}}_{ij}) &= \hat{O}_{2\alpha-1}(i, j; \hat{\mathbf{r}}_{ij}) \boldsymbol{\tau}_i \cdot \boldsymbol{\tau}_j, \end{aligned} \quad (2.2)$$

where  $\mathbf{S} \equiv \frac{1}{2}(\boldsymbol{\sigma}_i + \boldsymbol{\sigma}_j)$  is the total spin, and  $\mathbf{p}_{ij} = \frac{1}{2}(\mathbf{p}_i - \mathbf{p}_j)$  is the relative momentum operator of the pair of particles. In the following, we will also use the notation  $\alpha \in \{(cc), (c\tau), (\sigma c), (\sigma\tau), (Sc), (S\tau), (LSc), (LS\tau)\}$  for  $\alpha = 1-8$ . In neutron matter, the operators are projected to the isospin = 1 channel, i.e., we have

$$O_{\alpha}(i, j, \hat{\mathbf{r}}_{ij}) \rightarrow O_{\alpha}(i, j, \hat{\mathbf{r}}_{ij}) + O_{\alpha+1}(i, j, \hat{\mathbf{r}}_{ij}) \quad (2.3)$$

for odd  $\alpha$  and  $O_{\alpha}(i, j, \hat{\mathbf{r}}_{ij}) = 0$  for even  $\alpha$ . The new set of interaction channels will be  $\alpha \in \{(c), (\sigma), (S), (LS)\}$ .

The Argonne interaction [32] is, among others, formulated in the operator representation. For the  $v_8$  version of the Reid 68 interaction we have taken the six components  $V_{\alpha}^{(6)}(r)$ ,  $\alpha \in \{(cc), (c\tau), (\sigma c), (\sigma\tau), (Sc), (S\tau)\}$  from Eqs. (A3)–(A8) of Ref. [34]. The spin-orbit components  $\alpha \in \{(LSc), (LS\tau)\}$  were constructed [29], following the procedure of Ref. [32], from the isospin  $T = 0$  and isospin  $T = 1$  components of the Reid interaction; cf. Eqs. (20) and (30) of Ref. [30].

A somewhat more recent interaction [33] is given only in a partial wave representation. To derive an operator structure of the form (2.1) from the partial wave representation of the interaction we need the partial-wave representation of the operators  $\mathbf{L} \cdot \mathbf{S}$  and  $S_{12}$ . For neutron matter we only need the case  $T = 1$ . On the other hand, we need a definite total spin  $S = 0$  or  $S = 1$  for the pairing problem. The central components of the interaction are then

$$v_{c,0}(r) = v_c(r) - 3v_{\sigma}(r), \quad (2.4a)$$

$$v_{c,1}(r) = v_c(r) + v_{\sigma}(r). \quad (2.4b)$$

In the spin-singlet case we only have a central interaction and the only reasonable choice is

$$V(S = 0, T = 1)(r) \equiv V_{1S_0}(r) = v_{c,0}(r). \quad (2.5)$$

In the spin-triplet case, the operator structure is

$$\hat{V}(S = 1, T = 1)(r) = v_{c,1}(r)\mathbb{1} + v_S(r)\hat{S}_{12}(\mathbf{r}) + v_{LS}(r)\mathbf{L} \cdot \mathbf{S}, \quad (2.6)$$

where, for each partial wave, we have [36]

$$\mathbf{L} \cdot \mathbf{S} = \begin{pmatrix} j-1 & 0 \\ 0 & -j-2 \end{pmatrix} \quad (2.7)$$

and

$$S_{ij} = \begin{pmatrix} \frac{-2(j-1)}{2j+1} & \frac{6\sqrt{j(j+1)}}{2j+1} \\ \frac{6\sqrt{j(j+1)}}{2j+1} & \frac{-2(j+2)}{2j+1} \end{pmatrix}. \quad (2.8)$$

It is evidently impossible to represent all individual partial waves with only eight (or, in neutron matter, four) interaction components as required by the operator representation (2.1). We have therefore explored two possibilities, as follows, to define an operator representation of the Reid 93 potential. The tensor interaction is in both cases determined by the  ${}^3P_2$ - ${}^3F_2$  interaction,

$$v_S(r) = \frac{5}{6\sqrt{6}} V_{3P_2-{}^3F_2}(r). \quad (2.9)$$

- (i) If we want to reproduce the  ${}^3P_0$ - ${}^3P_0$  and the  ${}^3P_2$ - ${}^3P_2$  phase shifts, we get

$$v_{c,1}(r) = \frac{1}{3}(2V_{3P_2-{}^3P_2}(r) + V_{3P_0-{}^3P_0}(r)) + \frac{8}{5}v_S(r), \quad (2.10a)$$

$$v_{LS}(r) = \frac{1}{3}(V_{3P_2-{}^3P_2}(r) - V_{3P_0-{}^3P_0}(r)) - \frac{6}{5}v_S(r). \quad (2.10b)$$

- (ii) If we want to reproduce the  ${}^3P_2$ - ${}^3P_2$  and the  ${}^3F_2$ - ${}^3F_2$  phase shifts, we have

$$v_{c,1}(r) = \frac{1}{5}(4V_{3P_2-{}^3P_2}(r) + V_{3F_2-{}^3F_2}(r)) + \frac{16}{25}v_S(r), \quad (2.11a)$$

$$v_{LS}(r) = \frac{1}{5}(V_{3P_2-{}^3P_2}(r) - V_{3F_2-{}^3F_2}(r)) - \frac{6}{25}v_S(r). \quad (2.11b)$$

We shall refer to the approximations (2.10) and (2.11) as “Version a” and “Version b”, respectively. Turning the ambiguity into an advantage, we shall compare the results

from these two interaction models to assess the accuracy of predictions based on the operator representation of the Reid 93 interactions. For the body of this work we have chosen the operator form (2.10) that reproduces the lowest-lying partial waves. The equation of state obtained with this interaction is practically indistinguishable from the equation of state obtained from the Reid 68 and Argonne  $v_8$  potentials. Nevertheless, exploring different representations can provide insight into the robustness of theoretical predictions; see Appendix B.

We have focused in this paper on calculations for two variants of the Reid interaction [30,33] as well on the  $v_8$  truncation of the Argonne interaction [32]. This was done to be consistent with our previous work [17,27,28] as well as other microscopic calculations [37–40]. We are, of course, aware of the fact that there are more modern interactions [41,42] which have been used for the calculation of properties of neutron and nuclear matter [43–46]. The present paper focuses on  $P$ -wave pairing, whereas an investigation of these new interactions warrants a much broader investigation including other phenomena such as the structure [27],  $S$ -wave pairing [17], the dynamic structure [29], and the optical potential. We shall address these issues in future work.

## B. Jastrow-Feenberg variational method and parquet diagrams

In terms of the paradigms of perturbative many-body theory [47], it is easy to argue that the *minimum* set of Feynman diagrams for a trustworthy microscopic treatment of strongly interacting systems is the set of *parquet diagrams* [48,49]. While the insight into what is needed is quite obvious, the execution of such a program is far from trivial. One must seek approximations, but such steps are ambiguous without further guidance.

An approach that is superficially very different from perturbative many-body theory has been suggested by Jastrow [50] and Feenberg [51]. For simple, state-independent interactions as appropriate for electrons or quantum fluids, the Jastrow-Feenberg ansatz [50,51] for the wave function

$$\Psi_0 = F_N \Phi_0, \quad F_N = \prod_{\substack{i,j=1 \\ i < j}}^N f(r_{ij}) \quad (2.12)$$

and its logical generalization to multiparticle correlation functions has been extremely successful. Here,  $\Phi_0$  is a model state describing the statistics and, when appropriate, the geometry of the system. For fermions, it is normally taken as a Slater determinant. We will here use the generalization to Bardeen-Cooper-Schrieffer (BCS) states [14,17,52–56].

One of the reasons for the success of this method is that it provides an upper bound for the ground state energy

$$E_0 = \frac{\langle \Psi_0 | H | \Psi_0 \rangle}{\langle \Psi_0 | \Psi_0 \rangle}. \quad (2.13)$$

A singularly useful hierarchy of equations for the calculation of the energy expectation value (2.13) is the hypernetted-chain summation technique [57,58]; it is characterized by the fact that it allows, at every level of implementation, the unconstrained optimization of the correlations via the variational

principle

$$\frac{\delta E_0}{\delta f}(\mathbf{r}_i, \mathbf{r}_j) = 0. \quad (2.14)$$

The method is referred to as the (Fermi-)hypernetted-chain-Euler-Lagrange, (F)HNC-EL, procedure.

An important insight was that this procedure corresponds to a summation of a “local approximation” of the parquet diagrams [48,59,60]. This was proved first for bosons; some additional approximations are made in a Fermi system [56]. The variational problem (2.14) ensures that one uses the best approximation for the computational effort one is willing to spend. We shall therefore use the language of Jastrow-Feenberg and parquet diagrams interchangeably, in particular for the benefit of those readers who are less familiar with the former.

The situation is considerably more complicated for realistic nucleon-nucleon interactions of the form (2.1). A plausible generalization of the wave function (2.12) is the “symmetrized operator product (SOP)” [61,62]

$$\Psi_0^{\text{SOP}} = F_N^{\text{SOP}} \Phi_0, \quad F_N^{\text{SOP}} = \mathcal{S} \left[ \prod_{\substack{i,j=1 \\ i < j}}^N \hat{f}(i, j) \right], \quad (2.15)$$

where

$$\hat{f}(i, j) = \sum_{\alpha=1}^n f_{\alpha}(r_{ij}) \hat{O}_{\alpha}(i, j), \quad (2.16)$$

and  $\mathcal{S}$  stands for symmetrization. The symmetrization is necessary because the operators  $\hat{O}_{\alpha}(i, j)$  and  $\hat{O}_{\beta}(i, k)$  do not necessarily commute. We have highlighted recently [28] (see also Ref. [63]) the importance of a proper symmetrization in cases where the bare interaction is different in spin-singlet and spin-triplet channels; we shall return to this point in Sec. II B 3.

In a preceding series of papers [27–29], we developed practical and efficient methods for the summation of the parquet diagrams, including the most important commutator diagrams mentioned above. We shall briefly review the resulting equations in the next sections.

### 1. Diagram summation: Chain diagrams

One of the components of parquet-diagram theory is the summation of the chain diagrams. We assume a *local* effective particle-hole interaction of the same form as the bare interaction (2.1), which is given in momentum space as

$$\hat{V}_{\text{p-h}}(q) = \sum_{\alpha=1}^8 \tilde{V}_{\text{p-h}}^{(\alpha)}(q) \hat{O}_{\alpha}(i, j). \quad (2.17)$$

$\hat{V}_{\text{p-h}}(q)$  is, in the long-wavelength limit, related to Landau’s Fermi-Liquid interactions [64–66] or, at finite wave numbers, to pseudopotentials [8,67]. The momentum-space components of the interactions in the different operator channels are

the Fourier transforms

$$\tilde{V}_{p-h}^{(\alpha)}(q) = \begin{cases} \rho \int d^3r V_{p-h}^{(\alpha)}(r) j_0(qr) & \text{for } \alpha = 1, \dots, 4, \\ -\rho \int d^3r V_{p-h}^{(\alpha)}(r) j_2(qr) & \text{for } \alpha = 5, 6, \\ \frac{\rho}{2} \int d^3r V_{p-h}^{(\alpha)}(r) r k_F j_1(qr) & \text{for } \alpha = 7, 8, \end{cases} \quad (2.18)$$

where the momentum representation of the tensor operator is obtained by replacing  $\hat{r}_{ij} \rightarrow \hat{\mathbf{q}}$ . As usual, we have defined above the Fourier transforms with a density factor such that the momentum space interactions also have the dimension of energy.

The summation of chain diagrams is best carried out by transforming the spin and tensor operators into the longitudinal and transverse operators [68,69]. The particle-hole interaction is then a linear combination of the four operators

$$\hat{Q}_1 \equiv \mathbb{1}, \quad (2.19a)$$

$$\hat{Q}_3 \equiv \hat{L}(\hat{\mathbf{q}}) = (\boldsymbol{\sigma} \cdot \hat{\mathbf{q}})(\boldsymbol{\sigma}' \cdot \hat{\mathbf{q}}), \quad (2.19b)$$

$$\hat{Q}_5 \equiv \hat{T}(\hat{\mathbf{q}}) = \boldsymbol{\sigma} \cdot \boldsymbol{\sigma}' - (\boldsymbol{\sigma} \cdot \hat{\mathbf{q}})(\boldsymbol{\sigma}' \cdot \hat{\mathbf{q}}), \quad (2.19c)$$

$$\hat{Q}_7 \equiv \widetilde{\mathbf{L}} \cdot \mathbf{S} \equiv \frac{i}{k_F} \hat{\mathbf{q}} \times \Delta \mathbf{h} \cdot \mathbf{S}. \quad (2.19d)$$

The operator  $\widetilde{\mathbf{L}} \cdot \mathbf{S}$  acts only in spin space. It depends parametrically on the direction  $\hat{\mathbf{q}}$  of momentum transfer and the difference of the hole wave numbers  $\Delta \mathbf{h} \equiv \mathbf{h} - \mathbf{h}'$ . We shall generally mean the *momentum space* representations (2.19) when we refer to the operators  $\hat{Q}_\alpha$ .

A complete derivation of chain-diagram summations including the spin-orbit interaction was done in Ref. [29]. The sum of all chain diagrams can no longer be represented as a linear combination of momentum-space functions times the operators (2.19). Three more operators are needed. The coefficient functions of those additional operators that contain an even number of spin-orbit operators are, however, of order  $[\tilde{V}_{p-h}^{(LS)}(q)]^2$  and are numerically very small. An interesting feature of the spin-orbit order term, which might be relevant in different physical circumstances, will be outlined below in connection with Eqs. (2.22b)–(2.22d).

To represent the sum of all chain diagrams, it has turned out to be convenient to introduce

$$\tilde{V}_{p-h}^{(c)}(q; \omega) \equiv \tilde{V}_{p-h}^{(c)}(q) + \frac{1}{4} \chi_0^{(\perp)}(q; \omega) [\tilde{V}_{p-h}^{(LS)}(q)]^2, \quad (2.20a)$$

$$\tilde{V}_{p-h}^{(T)}(q; \omega) \equiv \tilde{V}_{p-h}^{(T)}(q) + \frac{1}{8} \chi_0^{(\perp)}(q; \omega) [\tilde{V}_{p-h}^{(LS)}(q)]^2, \quad (2.20b)$$

$$\tilde{V}_{p-h}^{(L)}(q; \omega) \equiv \tilde{V}_{p-h}^{(L)}(q). \quad (2.20c)$$

We have defined above a transverse Lindhard function

$$\chi_0^{(\perp)}(q; \omega) = \frac{1}{N} \text{Tr}_\sigma \sum_{\mathbf{h}} \left| \frac{\hat{\mathbf{q}} \times \mathbf{h}}{k_F} \right|^2 \frac{2(\varepsilon_p - \varepsilon_h)}{(\hbar\omega + i\eta)^2 - (\varepsilon_p - \varepsilon_h)^2}, \quad (2.21)$$

where  $\mathbf{q} = \mathbf{p} - \mathbf{h}$ . The  $\varepsilon_p$  and  $\varepsilon_h$  are the single-particle energies of correlated basis functions (CBF) theory that have been discussed elsewhere [70–72]; see also the Appendix of Ref. [17].

The sum of all chain diagrams containing an odd number of spin-orbit operators can be written as

$$\hat{W}_{LS}^{(\text{odd})}(\mathbf{q}; \omega) = W^{(LS)}(\mathbf{q}, \omega) \widetilde{\mathbf{L}} \cdot \mathbf{S} + W^{(LS')}(\mathbf{q}, \omega) \widetilde{\mathbf{L}} \mathbf{S}', \quad (2.22a)$$

$$W^{(LS)}(\mathbf{q}, \omega) = \frac{1}{2} \frac{\tilde{V}_{p-h}^{(LS)}(q)}{1 - \chi_0(q; \omega) \tilde{V}_{p-h}^{(c)}(q; \omega)} + \frac{1}{2} \frac{\tilde{V}_{p-h}^{(LS)}(q)}{1 - \chi_0(q; \omega) \tilde{V}_{p-h}^{(T)}(q; \omega)}, \quad (2.22b)$$

$$W^{(LS')}(\mathbf{q}, \omega) = \frac{1}{2} \frac{\tilde{V}_{p-h}^{(LS)}(q)}{1 - \chi_0(q; \omega) \tilde{V}_{p-h}^{(T)}(q; \omega)} - \frac{1}{2} \frac{\tilde{V}_{p-h}^{(LS)}(q)}{1 - \chi_0(q; \omega) \tilde{V}_{p-h}^{(c)}(q; \omega)}, \quad (2.22c)$$

where  $\chi_0(q; \omega)$  is the usual Lindhard function, and we deviate here slightly from the definition in Ref. [29],

$$\widetilde{\mathbf{L}} \mathbf{S}' = \frac{i}{2k_F} \hat{\mathbf{q}} \times (\mathbf{h} + \mathbf{h}') \cdot (\boldsymbol{\sigma} - \boldsymbol{\sigma}'). \quad (2.22d)$$

The operator  $\widetilde{\mathbf{L}} \mathbf{S}'$  is antisymmetric in the spins and does not contribute to the pairing interactions. In different physical circumstances the term proportional to  $\widetilde{\mathbf{L}} \mathbf{S}'$  could be very interesting because it is the only term in the effective interaction that couples spin-singlet and spin-triplet states.

The energy dependent effective interaction can then be represented by the operator expansion

$$\hat{W}(\mathbf{q}; \omega) = \sum_{\alpha \text{ odd}}^7 \tilde{W}^{(\alpha)}(q; \omega) \hat{Q}_\alpha, \quad (2.23)$$

where

$$\tilde{W}^{(\alpha)}(q; \omega) = \frac{\tilde{V}_{p-h}^{(\alpha)}(q; \omega)}{1 - \chi_0(q; \omega) \tilde{V}_{p-h}^{(\alpha)}(q; \omega)} \quad \text{for } \alpha = 1, 3, 5, \quad (2.24)$$

and Eq. (2.22b) for  $\alpha = 7$ .

## 2. Diagram summation: Ladder diagrams

The second component of the parquet [or (F)HNC-EL] summation is the summation of ladder diagrams. That is generally accomplished by the Bethe-Goldstone equation. In its most primitive form the equation contains, as the only many-body effect, the Pauli exclusion principle. Summing parquet diagrams amounts to supplementing the bare interaction  $v(r)$  by an “induced interaction”  $\tilde{w}_I(q, \omega)$ . This induced interaction is energy dependent. *Local* parquet theory then replaces this interaction by an energy-independent interaction which is defined such that the static approximation leads to the same (observable) static structure function as the dynamic

interaction:

$$\begin{aligned}
 S(q) &= - \int_0^\infty \frac{d\hbar\omega}{\pi} \text{Im} \frac{\chi_0(q; \omega)}{1 - \tilde{V}_{p-h}(q)\chi_0(q; \omega)} \\
 &= - \int_0^\infty \frac{d\hbar\omega}{\pi} \text{Im} [\chi_0(q; \omega) + \chi_0^2(q; \omega)\tilde{W}(q; \omega)] \\
 &\stackrel{!}{=} - \int_0^\infty \frac{d\hbar\omega}{\pi} \text{Im} [\chi_0(q; \omega) + \chi_0^2(q; \omega)\tilde{W}(q)], \quad (2.25)
 \end{aligned}$$

which defines the energy dependent induced interaction though

$$\tilde{W}(q, \omega) = \tilde{V}_{p-h}(q) + \tilde{w}_I(q, \omega) \quad (2.26)$$

and its local approximation

$$\tilde{W}(q) = \tilde{V}_{p-h}(q) + \tilde{w}_I(q). \quad (2.27)$$

The Bethe-Goldstone equation defines a pair wave function  $\psi(\mathbf{r})$  which can be identified, in the simplest case of central state-independent correlations and the FHNC//0 or parquet//0 approximation, with the “direct correlation function”  $\Gamma_{dd}(r)$  through

$$1 + \Gamma_{dd}(\mathbf{r}) = |\psi(\mathbf{r})|^2 \quad (2.28)$$

and is, in that approximation, related to the static structure function through

$$\tilde{\Gamma}_{dd}(\mathbf{q}) = \frac{S_F(q) - S(q)}{S_F^2(q)}. \quad (2.29)$$

Here,  $S_F(q)$  is the static structure function of noninteracting fermions. For the present case of interacting nucleons, all quantities are operators in the same basis as the microscopic interaction; see Refs. [27] and [73] for details. The resulting particle-hole interaction is

$$\begin{aligned}
 \hat{V}_{p-h}(\mathbf{r}) &= \frac{\hbar^2}{m} |\nabla \hat{\psi}(\mathbf{r})|^2 + \hat{\psi}^*(\mathbf{r})[\hat{v}(\mathbf{r}) \\
 &\quad + \hat{V}_I(\mathbf{r}) + \hat{w}_I(\mathbf{r})]\hat{\psi}(\mathbf{r}) - \hat{w}_I(r). \quad (2.30)
 \end{aligned}$$

The additional term  $\hat{V}_I(r)$  is the “irreducible” interaction which arises from the beyond-parquet contributions.

### 3. Diagram summation: Beyond parquet

The most notorious problem of an operator-dependent variational wave function (2.15) is that symmetrization must be carried out explicitly in order to get a valid variational principle (2.14). Light was shed on the meaning of the arising “commutator contributions” by Smith and Jackson [73], who showed, for a fictitious system of bosons with spin, isospin, and tensor forces, that the parquet-diagram summation leads to an optimized Bose-version of Ref. [61], i.e., to a theory where *all commutator diagrams are omitted*. The conclusion is therefore that the wave function (2.15) contains *more* than just the parquet class; nonparquet diagrams simply are neglected when commutators are neglected.

From the point of view of the variational wave function (2.15), it is abundantly clear that commutator diagrams are important whenever the interaction in singlet and triplet channels is very different: Working out the simplest nontrivial commutators leads to contributions to the energy where the

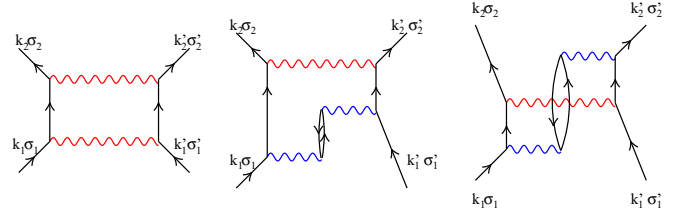


FIG. 1. The simplest second-order ladder diagrams including a “twisted chain” correction. The left diagram is the ordinary two-body ladder that is summed by the Bethe-Goldstone equation. The middle diagram is where one of the bare interactions is replaced by  $\tilde{w}_I(q)$ , and the right one is the simplest contribution to the totally irreducible interaction. The red wavy line represents the bare interaction and the blue wavy line the particle-hole interaction. The chains of two blue wavy lines may, of course, be supplemented by longer chains.

spin-singlet interaction is multiplied by a spin-triplet correlation function  $f_{\text{triplet}}(r)$  and vice versa. Taking the extreme case of hard-core interactions with different core sizes for singlet and triplet states [74], and simplistic correlations functions as they are being used in low-order constraint variational (LOCV) calculations, would lead to divergences.

The issue is less obvious in diagrammatic perturbation theory. But once the importance of non-parquet diagrams is realized, diagrammatic perturbation theory offers an intuitive explanation. We show in Fig. 1 the simplest possibility of “twisting” chain diagrams. The leftmost diagram is the ordinary second-order ladder diagram as summed by the Bethe-Goldstone equation. The middle diagram shows the simplest case where the bare interaction is replaced by the induced interaction  $\tilde{w}_I(q, \omega)$  or, in practice, its local approximation  $\tilde{w}_I(q)$ . In both cases, if a pair of particles enters with quantum numbers  $|\mathbf{k}_1, \mathbf{k}'_1, S\rangle$  then it remains in that spin configuration throughout the process.

The third diagram, although it has the same components, is by definition not a parquet diagram; it represents the simplest contribution to the irreducible interaction  $\hat{V}_I(r)$ . Working out the spin-flux, one obtains for that

$$\begin{aligned}
 (\Delta V_I)^{(2)}(k) &= \int \frac{d^3q}{(2\pi)^3 \rho} \frac{1}{E(k, q)} [\tilde{w}_{l,c}(q)\hat{V}(\mathbf{k} - \mathbf{q}) \\
 &\quad + \tilde{w}_{l,\sigma}(q)[2\tilde{V}_t(\mathbf{k} - \mathbf{q}) - \tilde{V}_s(\mathbf{k} - \mathbf{q})]P_t \\
 &\quad - 3\tilde{w}_{l,\sigma}(q)\tilde{V}_t(\mathbf{k} - \mathbf{q})P_s], \quad (2.31)
 \end{aligned}$$

where  $E(\mathbf{k}, \mathbf{q})$  is the energy denominator appropriate for the process, and we have extended second order chains to the full induced interaction. Also, we have here omitted the tensor- and spin-orbit force for brevity.

The first line in the expression (2.31) simply says that, if the induced interaction does not carry spin, then the spins of the interaction operator  $\hat{V}(\mathbf{k} - \mathbf{q})$  remain the same. The second line of (2.31) carries our message: If the induced interaction carries a spin, then the spin-triplet interaction will contribute to the spin-singlet component of the induced interaction. Similarly, the spin-singlet interaction contributes to the spin-triplet component of the induced interaction.

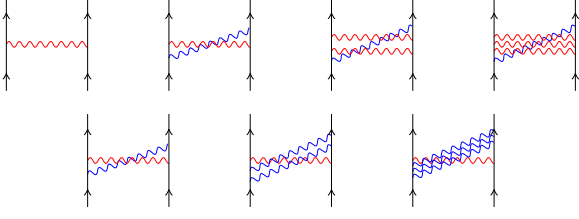


FIG. 2. Examples of the diagrams summed by the integral equation (2.32). The red wavy line represents a bare interaction  $\hat{v}(r)$  and the blue line represents the sum  $\hat{v} + \hat{w}_I$ . The rungs can all be summed to the  $G$  matrix.

We have developed a systematic way to sum the beyond-parquet diagrams in Ref. [28]. The  $G$  matrix of the Bethe-Goldstone equation  $\hat{G}(\mathbf{r})$  is the sum of the ladder-diagram summation of the bare interaction  $\hat{v}(\mathbf{r})$  plus the induced interaction  $\hat{w}_I(\mathbf{r})$ . A similar  $G$  matrix  $\hat{G}_w(\mathbf{r})$  can be defined for the local induced interaction  $w_I(\mathbf{r})$ . The irreducible interaction is then obtained by solving the integral equation

$$\begin{aligned} \hat{V}_I(\mathbf{q}) = & -\frac{1}{2} \sum_{\alpha,\beta} \int \frac{d^3q'}{(2\pi)^3\rho} [\tilde{G}^{(\alpha)}(|\mathbf{q}-\mathbf{q}'|) - \tilde{V}_I^{(\alpha)}(|\mathbf{q}-\mathbf{q}'|)] \\ & \times \frac{\tilde{G}_w^{(\beta)}(q')}{2t_F(q')} \times \text{Tr}_1[\hat{O}_\beta(a, 1)[\hat{O}_\alpha(a, b), \hat{O}_\beta(1, b)]], \end{aligned} \quad (2.32)$$

where  $\tilde{G}(\mathbf{q})$  is the Fourier transform of  $G(\mathbf{r})$ . The diagrams summed by this procedure are shown in Fig. 2.

### C. Superfluid state with correlations

We rely in this section heavily on definitions and methods of correlated basis functions (CBF) theory. The basic idea of a correlated BCS state is to use for the model state in Eq. (2.12) or (2.15) an uncorrelated BCS state. A *correlated* state is then constructed by applying a correlation operator (2.15) to that state. Since the superfluid state does not have a fixed particle number, we must write the correlated state in the form

$$|\text{CBCS}\rangle = \sum_{\mathbf{m}, N} |\Psi_{\mathbf{m}}^{(N)}\rangle \langle \mathbf{m}^{(N)} | \text{BCS}\rangle, \quad (2.33)$$

where the  $\{|\mathbf{m}^{(N)}\rangle\}$  form a complete set of  $N$ -body Slater determinants, and the  $|\Psi_{\mathbf{m}}^{(N)}\rangle$  are correlated and normalized  $N$ -body states forming a nonorthogonal basis of the Hilbert space:

$$|\Psi_{\mathbf{m}}^{(N)}\rangle = \frac{F_N |\mathbf{m}^{(N)}\rangle}{\langle \mathbf{m}^{(N)} | F_N^\dagger F_N | \mathbf{m}^{(N)} \rangle^{1/2}}. \quad (2.34)$$

The approach to deal with triplet pairing that is closest to ours is that of Hatzikonstantinou and Irvine [75] who generalized the work of Ref. [53] to pairing in triplet states. The uncorrelated wave function

$$|\text{BCS}\rangle = \prod_{\mathbf{k}} \left[ u(\mathbf{k}) + \sum_{\sigma_1\sigma_2} v_{\sigma_1\sigma_2}(\mathbf{k}) a_{\mathbf{k},\sigma_1}^\dagger a_{-\mathbf{k},\sigma_2}^\dagger \right] | \rangle \quad (2.35)$$

is the superposition of particle pairs in a spin-triplet state with opposite momenta. Above,  $u(\mathbf{k})$  is a normalization term.

In  $P$ -wave superconductivity [76], the superfluid system is frequently generated by a generalized Bogoliubov transformation

$$|\text{BCS}\rangle = e^{iS} | \rangle, \quad (2.36a)$$

$$\begin{aligned} iS = & \frac{1}{2} \sum_{\mathbf{k}, \sigma_1, \sigma_2} [\theta(\mathbf{k}, \sigma_1, \sigma_2) a_{\mathbf{k}, \sigma_1}^\dagger a_{-\mathbf{k}, \sigma_2}^\dagger \\ & - \theta^*(\mathbf{k}, \sigma_1, \sigma_2) a_{-\mathbf{k}, \sigma_2} a_{\mathbf{k}, \sigma_1}]. \end{aligned} \quad (2.36b)$$

The above unitary transformation defines quasiparticle operators [77]

$$\alpha_{\mathbf{k}} = e^{iS} \mathbf{a}_{\mathbf{k}} e^{-iS} = \mathbf{U}(\mathbf{k}) \mathbf{a}_{\mathbf{k}} - \mathbf{V}(\mathbf{k}) \mathbf{a}_{\mathbf{k}}^\dagger \quad (2.37)$$

where  $\mathbf{U}(\mathbf{k})$  and  $\mathbf{V}(\mathbf{k})$  are  $2 \times 2$  matrices and

$$\mathbf{a}_{\mathbf{k}} = \begin{pmatrix} a_{\mathbf{k}, \uparrow} \\ a_{\mathbf{k}, \downarrow} \end{pmatrix}. \quad (2.38)$$

The superfluid ground state is then the state that is annihilated by the quasiparticle destruction operators. We hasten to note that this state is not exactly the same as the state (2.34), the states deviate by a four-body term of the form  $a_{\mathbf{k}\uparrow}^\dagger a_{-\mathbf{k}\uparrow}^\dagger a_{\mathbf{k}\downarrow}^\dagger a_{-\mathbf{k}\downarrow}^\dagger$ . The relationship will be derived in Appendix A.

The theory has been worked out in detail and applied to nuclear problems by Tamagaki, Takatsuka, and collaborators [77, 78].

If the superfluid gap is small compared to the Fermi energy, it is legitimate to simplify the problem by expanding

$$\langle H' \rangle_c = \frac{\langle \text{CBCS} | \hat{H}' | \text{CBCS} \rangle}{\langle \text{CBCS} | \text{CBCS} \rangle}, \quad \hat{H}' \equiv \hat{H} - \mu \hat{N} \quad (2.39)$$

in the deviation of the superfluid values of  $u(\mathbf{k})$  and  $v_{\sigma_1\sigma_2}(\mathbf{k})$  from their normal states values  $u^{(0)}(\mathbf{k}) = 1 - n(k)$ ,  $v_{\sigma_1\sigma_2}^{(0)}(\mathbf{k}) = n(k) \delta_{\sigma_1\sigma_2}$ . Carrying out this expansion in the number of Cooper pairs, one arrives [53, 79] at a gap equation of exactly the same form as a mean-field approach, except that the pairing interaction is expressed as a sum of FHNC or parquet diagrams.

For pairing in states other than  $S$  waves, the gap function becomes angle dependent. We follow here the strategy of the ‘‘angle-average’’ approximation of the gap equation as formulated, for example, in Ref. [80]. In general, the gap equation can couple different angular momenta and becomes a matrix equation of the form

$$\Delta^{(\ell)}(k) = -\frac{1}{2} \sum_{\ell'} \int \frac{d^3k'}{(2\pi)^3} V_{\ell\ell'}(k, k') \frac{\Delta^{(\ell')}(k')}{\sqrt{(\varepsilon_{k'} - \mu)^2 + D^2(k')}} \quad (2.40)$$

where  $D^2(k) = \sum_{\ell} |\Delta^{(\ell)}(k)|^2$ . The pairing interaction has the form

$$\begin{aligned} V_{\ell\ell'}(k, k') = & \mathcal{W}_{\ell\ell'}(k, k') \\ & + (|\varepsilon_{\mathbf{k}} - \mu| + |\varepsilon_{\mathbf{k}'} - \mu|) \mathcal{N}_{\ell\ell'}(k, k'), \end{aligned} \quad (2.41)$$

$$\mathcal{W}_{\ell\ell'}(k, k') = \langle k, \ell | \mathcal{W}(1, 2) | k', \ell' \rangle, \quad (2.42)$$

$$\mathcal{N}_{\ell\ell'}(k, k') = \langle k, \ell | \mathcal{N}(1, 2) | k', \ell' \rangle, \quad (2.43)$$

where we have suppressed spin degrees of freedom because we are always working in either an  $S = 0$  or an  $S = 1$  state. The effective interaction  $\mathcal{W}(1, 2)$  and the correlation corrections  $\mathcal{N}(1, 2)$  are given by the compound-diagrammatic ingredients of the FHNC-EL method for off-diagonal quantities [81], or, in a different language, by parquet-diagram summations.

### III. RESULTS

Throughout our calculations, we have utilized a noninteracting single-particle spectrum  $\epsilon_k = \hbar^2 k^2 / 2m$ . One can go beyond such a simplifying approximation by either using the single-particle spectrum predicted by correlated basis functions theory [53] or improve upon that by including dynamic effects. These methods have been very successful for explaining the physical mechanisms leading to the strong effective mass enhancement in  ${}^3\text{He}$  [82], but applying them in the present case appeared excessive. The effective mass ratio  $m^*/m$  lies between 1.05 and 0.95 [83] and basically scales the gap, whereas, as we will see, the effect we are reporting can change the gap by two orders of magnitude.

As an initial exercise, and for completeness, we have solved the  $S$ -wave and  $P$ -wave gap equations for the bare interactions. We used the Reid 68 potential, the two operator versions of Reid 93, and the Argonne  $v_8$  potential. The results are discussed and compared with earlier work in Appendix B. To summarize the main conclusions:

- (i) The results for the  ${}^1S_0$  gap agree closely with each other, which gives confidence that the above interactions are well understood and leave only many-body effects to influence the magnitude of the gap. The temperature dependence is practically identical for the Reid 93 and Argonne  $v_8$  potentials.
- (ii) The results for the triplet pairing gap when many-body correlations are neglected are in full agreement with previous results [38,39,80], i.e., the diagonal  ${}^3P_2$  and off-diagonal  ${}^3P_2$ - ${}^3F_2$  pairing channels prevail in neutron matter, and the tensor interaction is essential. The temperature dependence is almost identical to that in the  ${}^1S_0$  channel.
- (iii) When the spin-orbit interaction is turned off, the  ${}^3P_2$  and  ${}^3P_2$ - ${}^3F_2$  gaps disappear. On the other hand,

turning off the spin-orbit interaction leads to a significant  ${}^3P_0$  gap for all interactions.

The question we address here is how many-body correlations modify the pairing interactions and the above-mentioned results for the pairing gaps.

#### A. Effective interactions

We have in Secs. II B 1–II B 3 formulated a version of the FHNC-EL or local parquet theory that retains, in the summation of chain diagrams, only the simplest exchange diagrams. This version has been dubbed FHNC-EL//0 or parquet//0. More complicated exchange diagrams are also important and routinely kept [27,28]; we refer to our previous publications [27–29] for details.

Input to our calculations of pairing gaps are our pairing matrix elements and the “energy numerator corrections” shown in Eq. (2.42). The latter might seem unfamiliar; discussion of the significance of this term is found in Refs. [84] and [83]. Basically, the formulation (2.40)–(2.42) amounts to a reformulation of the gap equation in terms of the  $T$  matrix as carried out, for example, in Ref. [85]. This reformulation is necessary to guarantee that the gap equation (2.40) has solutions in the limit of a contact interaction.

The straightforward application of the parquet-diagram summations would suggest taking, for the pairing interaction, the localized effective interactions (2.24) and (2.22b) which are made energy independent by the prescription (2.25). Since the gap is normally small compared to the kinetic energy of a particle at the Fermi surface, it is more appropriate to take these interactions at zero energy. We hasten to mention that the difference of results obtained in this way is negligible.

We focus in this work on  $P$ -wave pairing and assume an interaction in the operator representation (2.1). Examples of  $S$ -wave pairing can be seen in Appendix B. We can restrict ourselves to the  $T = 1$  case, i.e., the interaction contains only the four odd-numbered operators in Eq. (2.1). For the pairing problem, we need a definite total spin  $S = 0$  or  $S = 1$ . The central components of the interaction are then

$$v_{c,0}(r) = v_c(r) - 3v_\sigma(r), \quad (3.1a)$$

$$v_{c,1}(r) = v_c(r) + v_\sigma(r). \quad (3.1b)$$

For  ${}^3P_0$  pairing the interaction matrix (2.42) is diagonal,

$$V_{{}^3P_0}(p_1, p_2) = \int d^3r [v_{c,1}(r) - 4v_S(r) - 2v_{LS}(r)] j_1(p_1 r) j_1(p_2 r). \quad (3.2a)$$

For  ${}^3P_2$ - ${}^3F_2$  pairing we obtain a  $2 \times 2$  matrix with the elements

$$\begin{aligned} V_{{}^3P_2-{}^3P_2}(p_1, p_2) &= \int d^3r [v_{c,1}(r) - \frac{2}{5}v_S(r) + v_{LS}(r)] j_1(p_1 r) j_1(p_2 r), \\ V_{{}^3P_2-{}^3F_2}(p_1, p_2) &= \frac{6}{5}\sqrt{6} \int d^3r v_S(r) j_1(p_1 r) j_3(p_2 r), \\ V_{{}^3F_2-{}^3F_2}(p_1, p_2) &= \int d^3r [v_{c,1}(r) - \frac{8}{5}v_S(r) - 4v_{LS}(r)] j_3(p_1 r) j_3(p_2 r). \end{aligned} \quad (3.2b)$$

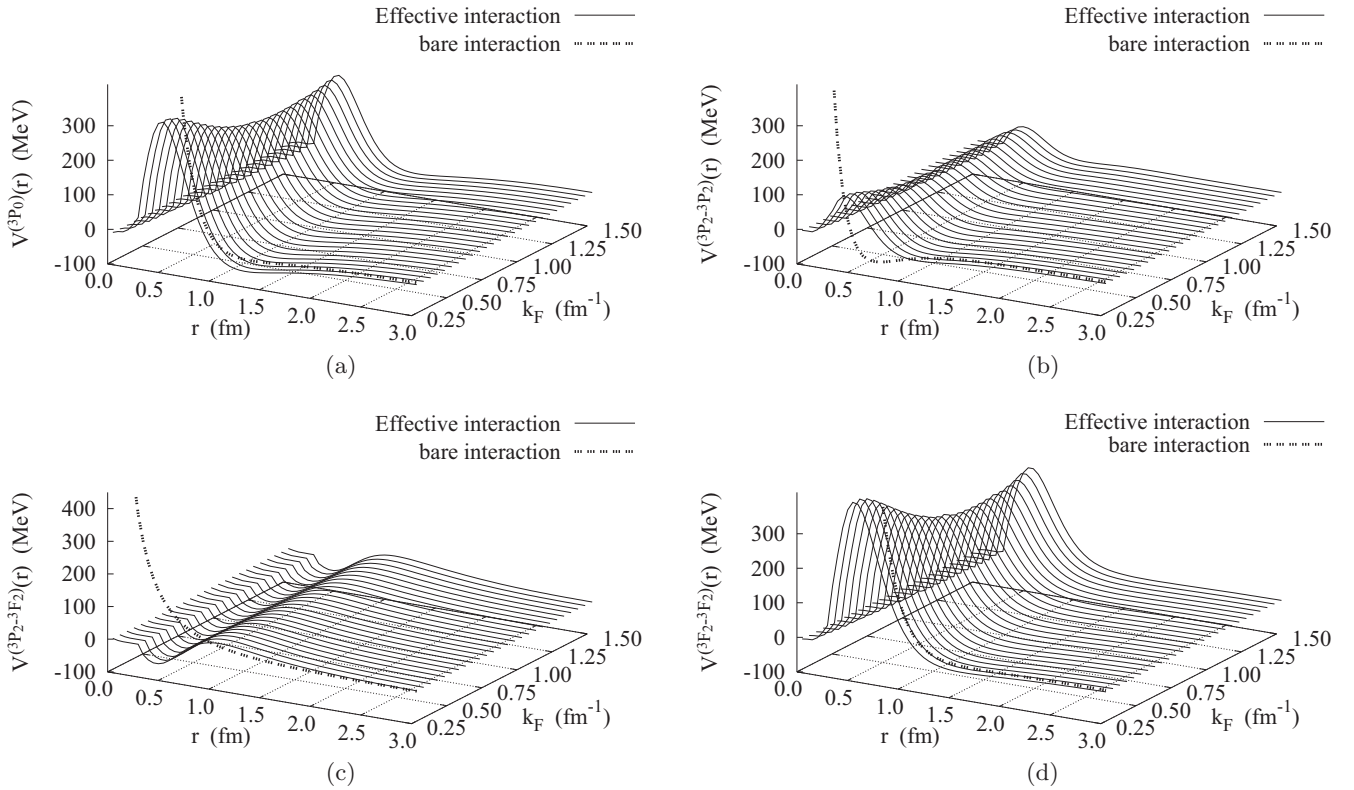


FIG. 3. For the Reid  $v_8$  interaction, the four effective interactions in (a) the  ${}^3P_0$ , (b) the  ${}^3P_2$ - ${}^3P_2$ , (c) the  ${}^3P_2$ - ${}^3F_2$ , and (d) the  ${}^3F_2$ - ${}^3F_2$  channels, for a sequence of Fermi wave number  $k_F$  values (solid lines). Also shown are the bare interactions in the same channels (heavy dashed lines).

The effective interaction  $\mathcal{W}(1,2)$  and the normalization correction  $\mathcal{N}(1,2)$  are originally represented in the same operator basis as the bare interaction; their matrix elements entering the gap equation are calculated according to Eqs. (3.2a)–(3.2b).

We show in Figs. 3 the effective interactions for the  $v_8$  version of the Reid 68 interaction in the  ${}^3P_0$  and the coupled  ${}^3P_2$ - ${}^3F_2$  coupled channels. Evidently there is not much similarity between the bare interactions and the effective interactions that contain medium-polarization, correlations, and “twisted” spin-exchange processes.

We found in Ref. [29] that the corrections to the effective interactions  $\tilde{W}^{(\alpha)}(q; \omega)$  for  $\alpha = 1, 3, 5$  due to the spin-orbit potential are very small. The only term that is of first order in the spin-orbit potential is  $\tilde{W}^{(7)}(q; \omega) = \tilde{W}^{(LS)}(q; \omega)$ . The most important result of that work is, however, the screening of the short-ranged behavior of the spin-orbit interaction by the correlations caused by the surrounding particles; see Fig. 4.

### B. ${}^3P_2$ - ${}^3F_2$ gaps

Figure 5 shows our final results for the superfluid  ${}^3P_2$ - ${}^3F_2$  gap function  $D(k_F)$ . Since the gap is negligibly small we did not dwell into technical details like the effect of “twisted chain” diagrams.

The most striking result is, of course, that, compared to the results with the bare interactions (Fig. 10), the  ${}^3P_2$ - ${}^3F_2$  is suppressed by about two orders of magnitude. The reason for this is readily found in the suppression of the spin-orbit interaction

through many-body correlations, as shown in Fig. 4. The special role of the spin-orbit interaction has already been pointed out in Ref. [5]: “without an attractive spin-orbit interaction, neutrons would form a  ${}^3P_0$  superfluid, in which the spin and orbital angular momenta are antialigned, rather than the  ${}^3P_2$  state, in which they are aligned.”

### C. ${}^3P_0$ gaps

Figure 6 shows our results for the superfluid  ${}^3P_0$  gap, omitting and including “beyond-parquet” corrections. We see a similar effect as observed in our work on  $S$ -wave pairing but

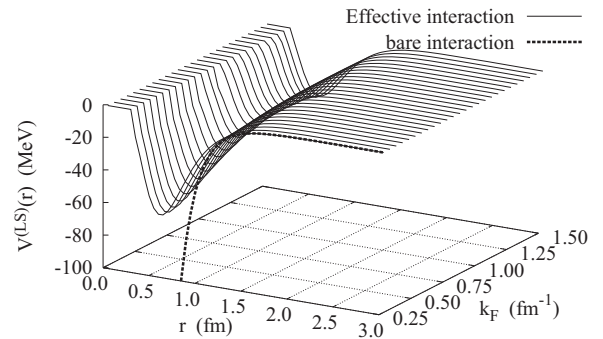


FIG. 4. For the Reid  $v_8$  interaction,  $W^{(LS)}(r; \omega = 0)$  for a sequence of Fermi wave number values  $k_F$ . Also shown is the bare spin-orbit interaction (heavy dashed line).

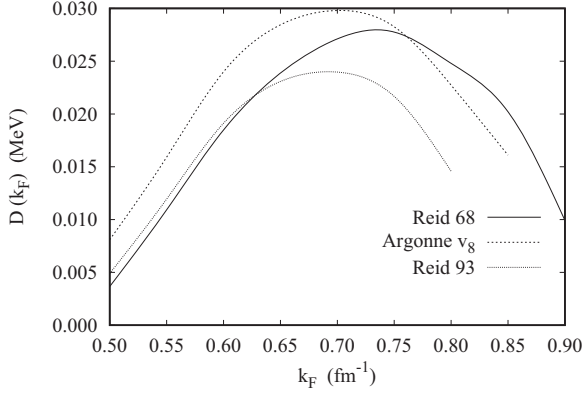


FIG. 5. Our results for the  ${}^3P_2$ - ${}^3F_2$  gap function  $D(k)$  for the Reid 68, Argonne  $v_8$ , and Reid 93a interactions.

with the opposite sign: Adding the “twisted chain” diagrams increases the  $P$ -wave gap by about 30%. This is plausible considering our discussion around Fig. 1. Adding “nonparquet” diagrams in the spin-singlet channel mixes the repulsive  $P$ -wave interaction into the  $S$ -wave pairing interaction. On the other hand, adding “nonparquet” diagrams in the spin-triplet channel mixes the attractive spin-singlet interaction to the spin-triplet pairing potential. We hasten to point out the effect is, however, rather delicate since the suppression of the spin-orbit potential depends sensitively on the balance between the central force and the spin-orbit force in the spin-triplet channels. It is less than the uncertainty introduced by using different microscopic potentials.

The fact that the “correlated wave function” ansatz (2.33) leads to a description of a superfluid system that can be understood as a weakly interacting theory with effective interactions permits us to generalize the description to finite temperatures. The gap equation then takes the form [86]

$$\Delta^{(\ell)}(k) = -\frac{1}{2} \sum_{\ell'} \int \frac{d^3k'}{(2\pi)^3} V_{\ell\ell'}(k, k') \times \frac{\tanh\left[\frac{1}{2}\beta E(k')\right]}{E(k')} \Delta^{(\ell')}(k'), \quad (3.3)$$

where  $\beta = 1/k_B T$  and  $E(k) = \sqrt{(\epsilon_k - \mu)^2 + D^2(k)}$ . Figure 7 shows the temperature dependence of the  ${}^3P_0$  gap for the Reid 68 interaction. In general, we find the relationship  $\Delta(k_F) \approx 1.8k_B T_c$  in very good agreement with the mean-field estimate  $\Delta(k_F) \approx 1.76k_B T_c$  [87], although the relationship

$$\Delta(k_F, T) \sim \left(1 - \frac{T}{T_c}\right)^{\frac{1}{2}} \quad (3.4)$$

is satisfied only close to the critical temperature  $T_c$ .

#### IV. SUMMARY AND OUTLOOK

Using several  $v_8$  models of the nucleon-nucleon interaction, we have calculated the effective pairing interaction in neutron matter by summing the parquet-diagrams and important totally irreducible corrections. In doing so, we have carried out the most comprehensive diagrammatic evaluation

of the pairing interactions, including, among others, medium polarization effects and spin-flip processes that have, so far, been either ignored or treated at a simplistic phenomenological level.

One can certainly do better. In particular, at high densities, more complicated exchange contributions can be relevant. These are routinely included in systems with simple interactions [71], but the summation techniques have not yet been developed for state-dependent potentials. Therefore, we have decided not to go beyond  $k_F = 1.8 \text{ fm}^{-1}$ .

The most striking result is that many-body correlations have the effect of almost completely suppressing the  ${}^3P_2$  and  ${}^3P_2$ - ${}^3F_2$  gap. This result was, to some extent, anticipated from our work on the spin-orbit interaction [29]. There, we found that the spin-orbit interaction is strongly suppressed by many-body correlations. It is also consistent with the fact that neither of the bare interactions employed here shows  ${}^3P_2$ - ${}^3F_2$  or  ${}^3P_2$  pairing when the spin-orbit interactions is omitted. Along with the suppression of  ${}^3P_2$ - ${}^3F_2$  pairing we found a significantly enhanced pairing in  ${}^3P_0$  states.

There are a number of obvious ways of extending our calculations. One of them is the inclusion of three-nucleon (3N) forces. Generally, the combined effect of 3N forces and in-medium mass normalization can vary strongly. A treatment of the three-nucleon interaction adjusted for applications in Brueckner-Hartree-Fock theory leads to a moderate increase near the peak [88]. On the other hand, the depletion of the Fermi surface can drastically reverse the effect [89]. In Ref. [25], it was found that a small fraction of the phenomenological repulsion of the original Urbana potential suffices to eliminate the gap. In the case of  $\chi$ EFT potentials, the contribution of the three-nucleon force at  $N^2$ LO and  $N^3$ LO is somewhat attractive, leading to an enhancement of the gap which is strongly regulator dependent [11,16], especially beyond Fermi momentum  $1.5 \text{ fm}^{-1}$ . Note that such momentum scales are close to the breakdown scale of  $\chi$ EFT.

Another potential extension of our work is to use a superfluid Lindhard function [90] for the calculation of the induced interaction. The effect can be quite large [17,56] in low-density neutron matter where the gap can be as large as half of the Fermi energy. We have not included these corrections here because the  ${}^3P_0$  gap is much smaller than the  ${}^1S_0$  gap and has its maximum at higher densities. In view of the approximations implicit to our parquet//1 calculation, we did not consider the effort justified.

#### APPENDIX A: UNITARY TRANSFORMATION

The Bogoliubov unitary transformation approach introduces a unitary operator [77,91]

$$\begin{aligned} iS &= \frac{1}{2} \sum_{\mathbf{k}, \sigma_1, \sigma_2} [\theta_{\sigma_1 \sigma_2}(\mathbf{k}) a_{\mathbf{k}\sigma_1}^\dagger a_{-\mathbf{k}\sigma_2}^\dagger - \theta_{\sigma_1 \sigma_2}^*(\mathbf{k}) a_{-\mathbf{k}\sigma_2} a_{\mathbf{k}\sigma_1}] \\ &\equiv \frac{1}{2} \sum_{\mathbf{k}} i s(\mathbf{k}), \end{aligned}$$

and, through that, a set of quasiparticle operators

$$\alpha_{\mathbf{k}} = e^{iS} \mathbf{a}_{\mathbf{k}} e^{-iS} = \mathbf{U}(\mathbf{k}) \mathbf{a}_{\mathbf{k}} - \mathbf{V}(\mathbf{k}) \mathbf{a}_{-\mathbf{k}}^\dagger, \quad (A1)$$

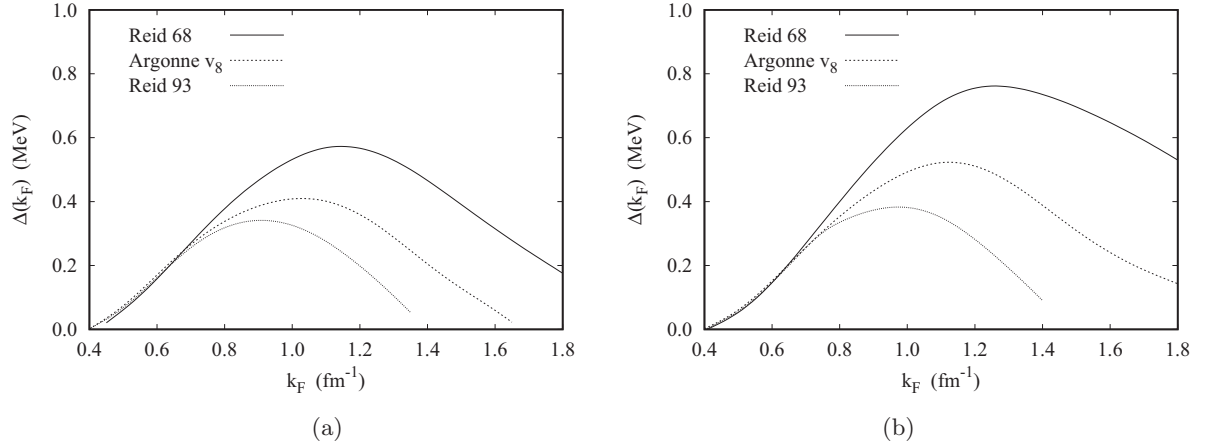


FIG. 6. For the three potentials considered here, the  ${}^3P_0$  gap is shown when (a) the “beyond parquet” diagrams are omitted and (b) when they are included.

where

$$\mathbf{a}_{\mathbf{k}} = \begin{pmatrix} a_{\mathbf{k}\uparrow}^\dagger \\ a_{\mathbf{k}\downarrow} \end{pmatrix} \quad (\text{A2})$$

and  $\mathbf{U}(\mathbf{k})$  and  $\mathbf{V}(\mathbf{k})$  are  $2 \times 2$  matrices.

In the spin-triplet case,  $\theta_{\sigma_1\sigma_2}(\mathbf{k})$  is symmetric, and we have  $\theta_{\sigma_1\sigma_2}(\mathbf{k}) = -\theta_{\sigma_1\sigma_2}(-\mathbf{k})$  as well as [78]  $\theta_{-\sigma_1-\sigma_2}^*(\mathbf{k}) = (-1)^{\sigma_1+\sigma_2}\theta_{\sigma_1\sigma_2}(\mathbf{k})$ , and we can write

$$iS = \sum_{\substack{\mathbf{k} \\ k_z > 0}} i s(\mathbf{k}). \quad (\text{A3})$$

Then all  $s(\mathbf{k})$  with different  $\mathbf{k}$  in the above sum commute. The matrices  $\mathbf{U}(\mathbf{k})$  and  $\mathbf{V}(\mathbf{k})$  have the form [78]

$$\mathbf{U}(\mathbf{k}) = \begin{pmatrix} u(\mathbf{k}) & 0 \\ 0 & u(\mathbf{k}) \end{pmatrix}, \quad \mathbf{V}(\mathbf{k}) = \begin{pmatrix} v(\mathbf{k}) & 0 \\ 0 & v(\mathbf{k}) \end{pmatrix} \theta(\mathbf{k}), \quad (\text{A4})$$

where  $u(\mathbf{k}) = \cos \theta_D(\mathbf{k})$ ,  $v(\mathbf{k}) = \sin \theta_D(\mathbf{k})/\theta_D(\mathbf{k})$ , and  $\theta_D(\mathbf{k}) = \sqrt{|\theta_{\uparrow\uparrow}(\mathbf{k})|^2 + |\theta_{\uparrow\downarrow}(\mathbf{k})|^2}$ . Conventionally, the Hamiltonian is rewritten in terms of the quasiparticle operators; the amplitudes  $u(\mathbf{k})$  and  $\theta_{\sigma_1\sigma_2}(\mathbf{k})$  are determined

by the condition that the off-diagonal part of the Hamiltonian in terms of the quasiparticle operators vanishes. For the execution of the variational/parquet theory outlined in Sec. II C we need, however, a closed-form expression for the uncorrelated state |BCS).. One definition is to demand that this state is destroyed by the quasiparticle annihilation operators,

$$\alpha_{\mathbf{k}}|\text{BCS}\rangle = 0. \quad (\text{A5})$$

It is immediately seen that such a condition cannot be satisfied by the form (2.34) and the quasiparticle operators (A2). Rather, the form of the wave function is

$$|\text{BCS}\rangle = \prod_{\substack{\mathbf{k} \\ k_z > 0}} F(\mathbf{k}), \quad (\text{A6})$$

$$F(\mathbf{k}) = A(\mathbf{k}) + \sum_{\sigma_1\sigma_2} B_{\sigma_1\sigma_2}(\mathbf{k}) a_{\mathbf{k}\sigma_1}^\dagger a_{-\mathbf{k}\sigma_2}^\dagger + C(\mathbf{k}) a_{\mathbf{k}\uparrow}^\dagger a_{-\mathbf{k}\uparrow}^\dagger a_{\mathbf{k}\downarrow}^\dagger a_{-\mathbf{k}\downarrow}^\dagger, \quad (\text{A7})$$

where the coefficients  $A(\mathbf{k})$ ,  $B_{\sigma_1\sigma_2}(\mathbf{k})$ , and  $C(\mathbf{k})$  are determined by the condition

$$\sum_{\sigma'} [U_{\sigma,\sigma'}(\mathbf{k}) a_{\mathbf{k},\sigma'} - V_{\sigma,\sigma'}(\mathbf{k}) a_{-\mathbf{k},\sigma'}^\dagger] F(\mathbf{k}) = 0 \quad (\text{A8})$$

and normalization. The first condition is that there are no terms proportional to  $a_{-\mathbf{k},\sigma}^\dagger$ . This leads to

$$u(\mathbf{k}) B_{\sigma\sigma'}(\mathbf{k}) = A(\mathbf{k}) V_{\sigma\sigma'}(\mathbf{k}). \quad (\text{A9})$$

The second condition is that the coefficients of three creation operators should also vanish.

$$\begin{aligned} & -C(\mathbf{k}) [U_{\sigma\uparrow} a_{\mathbf{k},\downarrow}^\dagger - U_{\sigma\downarrow} a_{\mathbf{k},\uparrow}^\dagger] \\ & - \sum_{\sigma_1} [V_{\sigma\uparrow}(\mathbf{k}) B_{\sigma_1\downarrow}(\mathbf{k}) - V_{\sigma\downarrow}(\mathbf{k}) B_{\sigma_1\uparrow}(\mathbf{k})] a_{\mathbf{k},\sigma_1}^\dagger \\ & = -[u(\mathbf{k}) C(\mathbf{k}) - [V_{\uparrow\uparrow}(\mathbf{k}) B_{\downarrow\downarrow}(\mathbf{k}) - V_{\uparrow\downarrow}(\mathbf{k}) B_{\downarrow\uparrow}(\mathbf{k})]] \\ & \quad \times [\delta_{\sigma\uparrow} a_{\mathbf{k},\downarrow}^\dagger - \delta_{\sigma\downarrow} a_{\mathbf{k},\uparrow}^\dagger]. \end{aligned} \quad (\text{A10})$$

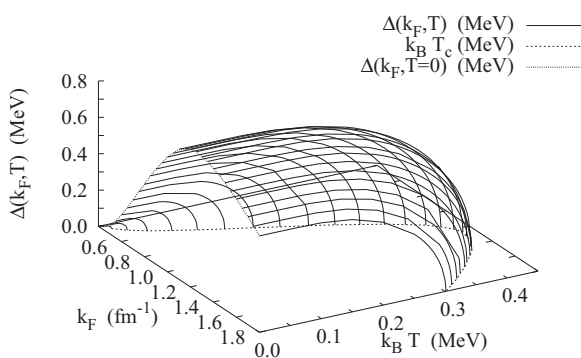


FIG. 7. For the Reid 68 interaction, the temperature dependence of the  ${}^3P_0$  gap. Also shown are the critical temperature  $T_c$  as a function of density [dashed line in the  $(k_F, k_B T)$  plane] and the zero temperature solution [dotted line in the  $(k_F, \Delta(k_F))$  plane].

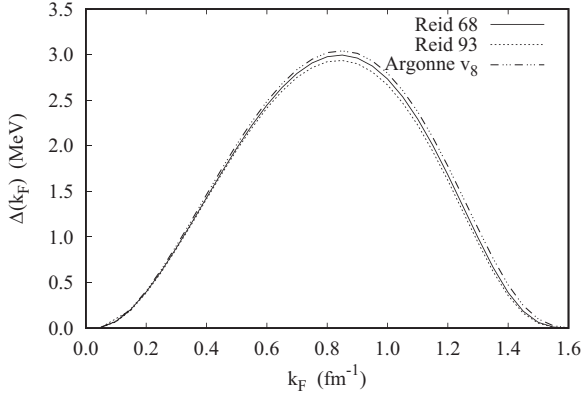


FIG. 8. The  $^1S_0$  gap for the operator form of the Reid 68, Reid 93, and Argonne  $v_8$  potentials. The two operator versions of Reid-93 give the same result.

Together with the normalization condition  $\langle |F^\dagger(\mathbf{k})F(\mathbf{k})| \rangle = 1$  this gives the result

$$F(\mathbf{k}) = u^2(\mathbf{k}) + u(\mathbf{k}) \sum_{\sigma_1 \sigma_2} V_{\sigma_1 \sigma_2}(\mathbf{k}) a_{\mathbf{k} \sigma_1}^\dagger a_{-\mathbf{k} \sigma_2}^\dagger + (u^2(\mathbf{k}) - 1) a_{\mathbf{k} \uparrow}^\dagger a_{-\mathbf{k} \uparrow}^\dagger a_{\mathbf{k} \downarrow}^\dagger a_{-\mathbf{k} \downarrow}^\dagger. \quad (\text{A11})$$

With that, the wave function is

$$|\text{BCS}\rangle = \prod_{\mathbf{k}} \prod_{k_z > 0} \left[ u^2(\mathbf{k}) + u(\mathbf{k}) \sum_{\sigma_1, \sigma_2} V_{\sigma_1, \sigma_2}(\mathbf{k}) a_{\mathbf{k}, \sigma_1}^\dagger a_{-\mathbf{k}, \sigma_2}^\dagger + (u^2(\mathbf{k}) - 1) a_{\mathbf{k} \uparrow}^\dagger a_{-\mathbf{k} \uparrow}^\dagger a_{\mathbf{k} \downarrow}^\dagger a_{-\mathbf{k} \downarrow}^\dagger \right] | \rangle. \quad (\text{A12})$$

Thus, the ‘‘unitary transformation’’ leads to a BCS state that also contains four creation operators. Such a term is, of course, irrelevant if the Hamiltonian just contains one- and two-body operators. It might lead to interesting effects once one goes beyond mean-field approximations.

## APPENDIX B: RESULTS WITH BARE INTERACTIONS

To examine the dependence of the results for the superfluid gap on the potential model and also to compare with earlier calculations [38,39,80], we have calculated  $\Delta(k_F)$  for the four potentials studied here. An aspect of concern is that most accurate nuclear interactions [30,33] are given in a partial wave basis, and an operator form, Eqs. (2.1) and (2.2), is an approximation. We have described above how the operator form of the Reid 93 interaction was obtained.

Figure 8 shows a comparison of the  $^1S_0$  gap obtained for the above three interaction models. The close agreement between these results gives confidence that these interactions are well understood, leaving only many-body effects to influence the magnitude of the gap.

Extending the calculation to finite temperature [86,87,92] also gives an estimate of the critical temperature  $T_c$ . Close to the transition temperature, one expects a behavior of the form (3.4).

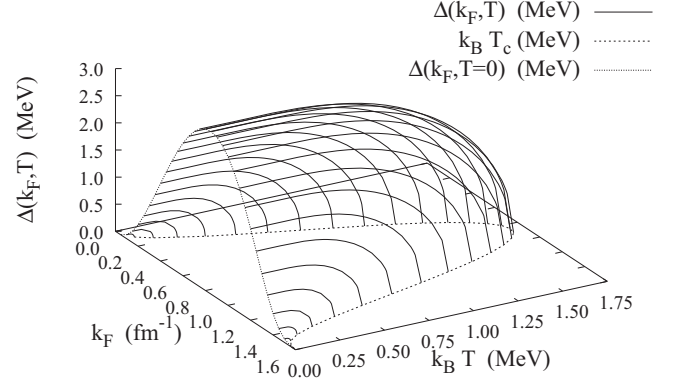


FIG. 9. For the Reid 68 interaction, the temperature dependence of the  $^1S_0$  gap. Also shown are the critical temperature  $T_c$  as a function of density (dashed line) in the  $(k_F, k_B T)$  plane and the zero temperature solution [dotted line in the  $(k_F, \Delta(k_F))$  plane].

We have calculated the temperature dependence of the  $^1S_0$  gap (see Fig. 9); the critical temperature was obtained by extrapolating the temperature dependence  $\Delta(k_F, T)$  to  $\Delta(k_F, T_c) = 0$  using the estimate (3.4). Our results are shown in Fig. 9. We found, to a very good approximation, that  $\Delta(k_F) \approx 1.8 k_B T_c$  throughout the whole density regime. This is in excellent agreement with the weak coupling approximation Eq. (51.44) of Ref. [87]. Results for the Argonne and Reid 93 interactions are practically identical.

The situation is more complex for  $P$ -wave pairing. The pioneering work of Tamagaki *et al.* [77,78] showed that, when many-body effects are neglected,  $^3P_2$  and  $^3P_2$ - $^3F_2$  prevail in neutron matter. The results that we have obtained for the interactions considered here fully support this view. Moreover, our results are rather similar for all four cases; see Fig. 10. We also found that, in the  $^3P_2$ - $^3F_2$  coupled channel pairing, the interactions in the  $^3P_2$ - $^3P_2$  diagonal and the  $^3P_2$ - $^3F_2$  off-diagonal (tensor) channel are most important whereas the diagonal  $^3F_2$ - $^3F_2$  interaction plays only a minor role. On the other hand, the off-diagonal tensor force is essential; restricting the

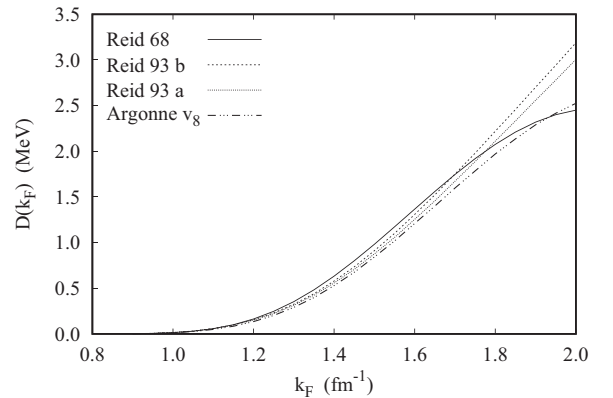


FIG. 10. The superfluid coupled channel  $^3P_2$ - $^3F_2$  gap for the four interactions considered here.  $D(k_F)$  is the angle-averaged gap function in the denominator of Eq. (2.40).

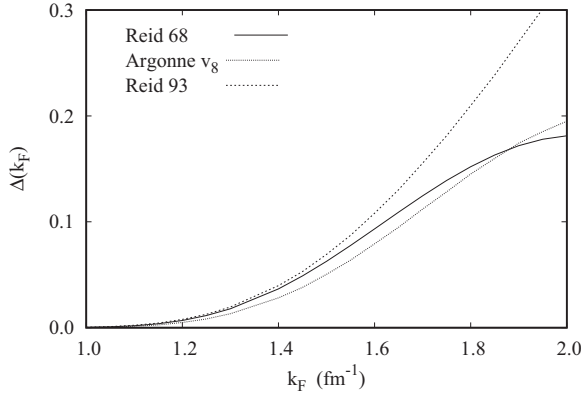


FIG. 11. The superfluid gap for  ${}^3P_2$  single channel. The two versions of the Reid 93 interaction give by construction the same answer.

calculation to the  ${}^3P_2$  channel reduces the gap by an order of magnitude; see Fig. 11.

The temperature dependence of the  ${}^3P_2$ - ${}^3F_2$  gap is almost identical to that of the  ${}^1S_0$  gap; see Fig. 12. In particular, we found again that the relationship  $\Delta(k_F) \approx 1.8k_B T_c$  with very good accuracy.

The calculations discussed so far did not necessarily rely on an operator structure of the form in Eqs (2.1) and (2.2). To assess the importance of the spin-orbit interaction we have repeated our calculations with the spin-orbit interaction turned off. As predicted [5], pairing in  ${}^3P_2$ - ${}^3F_2$  and  ${}^3P_2$  states disappeared apart from a tiny effect of  $10^{-2}$  MeV for  ${}^3P_2$  pairing with the Reid 68 interaction.

On the other hand, turning off the spin-orbit interaction leads to a significant  ${}^3P_0$  gap for all interactions considered here; see Fig. 13. Unlike all other cases, we observe a rather significant dependence of the value of  $\Delta(k_F)$  on the interaction. This simply reflects the ambiguity arises from the very definition of an operator structure of the interaction. In particular, the predictions of the two operator representations (2.10) and (2.11) of the Reid 93 interaction differ by more than a factor of 2.

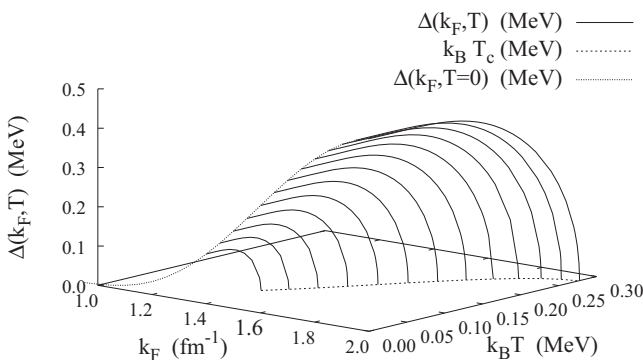


FIG. 12. Same as Fig. 9 for  ${}^3P_2$ - ${}^3F_2$  pairing.

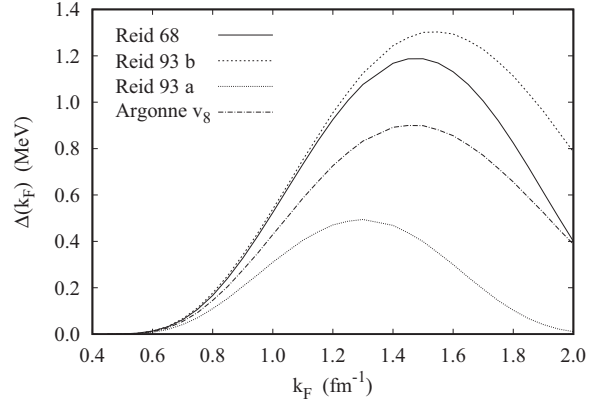


FIG. 13. The pairing gap in  ${}^3P_0$  states for the four interactions considered here when the spin-orbit force has been turned off.

### APPENDIX C: GAP EQUATION SOLVER

We describe here the version of our gap-equation solver [93] for finite temperatures. For brevity and in view of what follows, let

$$E_n(k, \xi) \equiv \sqrt{(\varepsilon_k - \mu)^2 + \xi^2 D_n^2(k)}. \quad (\text{C1})$$

Equations (3.3) and (2.40) are highly nonlinear and a simple iteration procedure of the kind

$$\begin{aligned} \Delta_{n+1}^{(\ell)}(k) = & -\frac{1}{2} \sum_{\ell'} \int \frac{d^3k'}{(2\pi)^3} V_{\ell\ell'}(k, k') \\ & \times \frac{\tanh\left(\frac{1}{2}\beta E_n(k', 1)\right)}{E_n(k', 1)} \Delta_n^{(\ell')}(k') \end{aligned} \quad (\text{C2})$$

normally does not converge. The reason for this is as follows: The function

$$\frac{\tanh\left[\frac{1}{2}\beta E_n(k', 1)\right]}{E_n(k', 1)}$$

is everywhere apart from a small area around  $k_F$  dominated by the kinetic energy  $|\varepsilon_{k'} - \mu|$ . We can therefore write (applying the mean value theorem)

$$\begin{aligned} \Delta_{n+1}^{(\ell)}(k) = & -\frac{1}{2} \sum_{\ell'} \int \frac{d^3k'}{(2\pi)^3} V_{\ell\ell'}(k, k') \\ & \times \frac{\tanh\left(\frac{1}{2}\beta\sqrt{(\varepsilon_{k'} - \mu)^2 + \bar{D}^2(k_F)}\right)}{\sqrt{(\varepsilon_{k'} - \mu)^2 + \bar{D}^2(k_F)}} \Delta_n^{(\ell')}(k'), \end{aligned} \quad (\text{C3})$$

where  $\bar{D}(k_F)$  is an average value of the gap function  $D(k)$  in the vicinity of  $k_F$ . This procedure converges towards the eigenvector corresponding to the *largest eigenvalue in absolute value* of the matrix

$$-\frac{1}{2} V_{\ell\ell'}(k, k') \frac{\tanh\left(\frac{1}{2}\beta\sqrt{(\varepsilon_{k'} - \mu)^2 + \bar{D}^2(k_F)}\right)}{\sqrt{(\varepsilon_{k'} - \mu)^2 + \bar{D}^2(k_F)}}.$$

However, if the interaction has a strong repulsive core, the above operator has very large *negative* eigenvalues whereas we *want* the largest positive eigenvalue.

A very rapidly converging algorithm [93] is as follows: Consider the generalized eigenvalue problem

$$\lambda(\xi)\delta_{n+1}^{(\ell)}(k, \xi) = -\frac{1}{2} \sum_{\ell'} \int \frac{d^3k'}{(2\pi)^3} V_{\ell\ell'}(k, k') \times \frac{\tanh\left(\frac{1}{2}\beta E_n(k', \xi)\right)}{E_n(k', \xi)} \delta_{n+1}^{(\ell')}(k', \xi), \quad (\text{C4})$$

where  $\xi$  is a scaling parameter. The eigenvectors are normalized as

$$\sum_{\ell} \int \frac{d^3k}{(2\pi)^3} \frac{1}{2} \frac{\tanh\left(\frac{1}{2}\beta E_n(k, \xi)\right)}{E_n(k, \xi)} |\delta_{n+1}^{(\ell)}(k)|^2 = 1. \quad (\text{C5})$$

The algorithm is

- (1) Start with a reasonable estimate for  $D_0(k)$ . From the above analysis we can expect that a constant is a good approximation.
- (2) Solve the above eigenvalue problem as a function of the scaling parameter  $\xi$ , and find the value  $\xi_0$  for which an eigenvalue of the equation is  $\lambda(\xi_0) = 1$ . The

derivative is

$$\begin{aligned} \frac{d \ln \lambda(\xi)}{d\xi} &= \sum_{\ell} \int \frac{d^3k}{(2\pi)^3} |\delta_{n+1}^{(\ell)}(k)|^2 \frac{d}{d\xi} \\ &\quad \times \frac{\tanh\left[\frac{1}{2}\beta E_n(k, \xi)\right]}{E_n(k, \xi)} \\ &= -\xi \sum_{\ell} \int \frac{d^3k}{(2\pi)^3} \left| \frac{D_n(k)\delta_{n+1}^{(\ell)}(k)}{E_n(k, \xi)} \right|^2 \\ &\quad \times \frac{\tanh\left[\frac{1}{2}\beta E_n(k, \xi)\right]}{E_n(k, \xi)} \\ &\quad \times \left[ 1 - \frac{\beta E_n(k, \xi)}{\sinh[\beta E_n(k, \xi)]} \right] < 0 \quad (\text{C6}) \end{aligned}$$

for  $\lambda > 0$ . This feature is useful to find the value  $\xi_0$  by a Newton procedure.

- (3) Scale the corresponding eigenfunction  $\delta_{n+1}^{(\ell)}(k, \xi_0)$  such that

$$D_{n+1}(k) = \delta_{n+1}(k, \xi_0) \frac{\xi_0 D_n(k_F)}{\delta_{n+1}(k_F, \xi_0)}.$$

- (4) Go to step (2) and repeat until convergence which is reached for  $\xi_0 = 1$ .

It was already observed in Ref. [93] and confirmed in Ref. [80] that the first iteration often leads to a solution of the gap equation with a percent accuracy. We have confirmed this observation here. A stand-alone code together with a brief description on how it works are provided as Supplemental Material [94].

- 
- |   |  |
|---|--|
| <p>[1] A. Bohr, B. R. Mottelson, and D. Pines, <i>Phys. Rev.</i> <b>110</b>, 936 (1958).</p> <p>[2] D. J. Dean and M. Hjorth-Jensen, <i>Rev. Mod. Phys.</i> <b>75</b>, 607 (2003).</p> <p>[3] D. Page and S. Reddy, <i>Annu. Rev. Nucl. Part. Sci.</i> <b>56</b>, 327 (2006).</p> <p>[4] R. Broglia and V. Zelevinsky, <i>Fifty Years of Nuclear BCS</i> (World Scientific, Singapore, 2013).</p> <p>[5] A. Gezerlis, C. J. Pethick, and A. Schwenk, in <i>Novel Superfluids</i>, edited by K. H. Bennemann and J. B. Ketterson (Oxford University Press, Oxford, 2014), Vol. 2, Chap. 22, pp. 580–615.</p> <p>[6] D. Page, J. M. Lattimer, M. Prakash, and A. W. Steiner, in <i>Novel Superfluids</i>, edited by K.-H. Bennemann and J. B. Ketterson (Oxford University Press, Oxford, 2015), Vol. 2, Chap. 21, p. 505–579.</p> <p>[7] L. N. Cooper, R. L. Mills, and A. M. Sessler, <i>Phys. Rev.</i> <b>114</b>, 1377 (1959).</p> <p>[8] J. Wambach, T. Ainsworth, and D. Pines, <i>Nucl. Phys. A</i> <b>555</b>, 128 (1993).</p> <p>[9] J. W. Clark, in <i>Fifty Years of Nuclear BCS</i>, edited by R. A. Broglia and V. Zelevinsky (World Scientific, Singapore, 2013), Chap. 27, pp. 360–376.</p> <p>[10] G. E. Pavlou, E. Mavrommatis, C. Moustakidis, and J. W. Clark, <i>Eur. Phys. J. A</i> <b>53</b>, 96/1 (2017).</p> <p>[11] A. Rios, A. Polls, and W. H. Dickhoff, <i>J. Low Temp. Phys.</i> <b>189</b>, 234 (2017).</p> | <p>[12] O. Benhar and G. D. Rosi, <i>J. Low Temp. Phys.</i> <b>189</b>, 250 (2017).</p> <p>[13] A. Schwenk, B. Friman, and G. E. Brown, <i>Nucl. Phys. A</i> <b>713</b>, 191 (2003).</p> <p>[14] A. Fabrocini, S. Fantoni, A. Y. Illarionov, and K. E. Schmidt, <i>Phys. Rev. Lett.</i> <b>95</b>, 192501 (2005).</p> <p>[15] L. G. Cao, U. Lombardo, and P. Schuck, <i>Phys. Rev. C</i> <b>74</b>, 064301 (2006).</p> <p>[16] C. Drischler, T. Krüger, K. Hebeler, and A. Schwenk, <i>Phys. Rev. C</i> <b>95</b>, 024302 (2017).</p> <p>[17] E. Krotscheck and J. Wang, <i>Phys. Rev. C</i> <b>103</b>, 035808 (2021).</p> <p>[18] Y. Lim and J. W. Holt, <i>Phys. Rev. C</i> <b>103</b>, 025807 (2021).</p> <p>[19] D. G. Yakovlev and P. Haensel, <i>Astron. Astrophys.</i> <b>407</b>, 259 (2003).</p> <p>[20] T. Takatsuka and R. Tamagaki, <i>Prog. Theor. Phys. Suppl.</i> <b>112</b>, 27 (1993).</p> <p>[21] O. Elgarøy, L. Engvik, M. Hjorth-Jensen, and E. Osnes, <i>Nucl. Phys. A</i> <b>607</b>, 425 (1996).</p> <p>[22] D. Ding, A. Rios, H. Dussan, W. H. Dickhoff, S. J. Witte, A. Carbone, and A. Polls, <i>Phys. Rev. C</i> <b>94</b>, 025802 (2016).</p> <p>[23] E. Krotscheck, P. Papakonstantinou, and J. Wang, <i>Astrophys. J.</i> <b>955</b>, 76 (2023).</p> <p>[24] L. Yuan, Three-body pairing interaction effect on superfluidity with applications to neutron star matter, Ph.D. thesis, Washington University, St. Louis, 2007 (unpublished).</p> <p>[25] P. Papakonstantinou and J. W. Clark, <i>J. Low Temp. Phys.</i> <b>189</b>, 361 (2017).</p> |
|---|--|

- [26] A. Schwenk and B. Friman, *Phys. Rev. Lett.* **92**, 082501 (2004).
- [27] E. Krotscheck and J. Wang, *Phys. Rev. C* **101**, 065804 (2020).
- [28] E. Krotscheck and J. Wang, *Phys. Rev. C* **102**, 064305 (2020).
- [29] E. Krotscheck and J. Wang, *Phys. Rev. C* **105**, 034345 (2022).
- [30] R. V. Reid, Jr., *Ann. Phys. (NY)* **50**, 411 (1968).
- [31] H. A. Bethe and M. B. Johnson, *Nucl. Phys. A* **230**, 1 (1974).
- [32] R. B. Wiringa, V. G. J. Stoks, and R. Schiavilla, *Phys. Rev. C* **51**, 38 (1995).
- [33] V. G. J. Stoks, R. A. M. Klomp, C. P. F. Terheggen, and J. J. de Swart, *Phys. Rev. C* **49**, 2950 (1994).
- [34] B. D. Day, *Phys. Rev. C* **24**, 1203 (1981).
- [35] R. B. Wiringa, R. A. Smith, and T. L. Ainsworth, *Phys. Rev. C* **29**, 1207 (1984).
- [36] M. Naghdi, *Phys. Part. Nuclei* **45**, 924 (2014).
- [37] J. M. C. Chen, J. W. Clark, R. D. Davé, and V. V. Khodel, *Nucl. Phys. A* **555**, 59 (1993).
- [38] V. A. Khodel, V. V. Khodel, and J. W. Clark, *Nucl. Phys. A* **598**, 390 (1996).
- [39] V. V. Khodel, V. A. Khodel, and J. W. Clark, *Nucl. Phys. A* **679**, 827 (2001).
- [40] M. Baldo, A. Polls, A. Rios, H.-J. Schulze, and I. Vidaña, *Phys. Rev. C* **86**, 064001 (2012).
- [41] E. Epelbaum, H.-W. Hammer, and Ulf-G. Meißner, *Rev. Mod. Phys.* **81**, 1773 (2009).
- [42] R. Machleidt and D. R. Entern, *Phys. Rep.* **503**, 1 (2011).
- [43] A. Gezerlis, I. Tews, E. Epelbaum, S. Gandolfi, K. Hebeler, A. Nogga, and A. Schwenk, *Phys. Rev. Lett.* **111**, 032501 (2013).
- [44] J. E. Lynn, J. Carlson, E. Epelbaum, S. Gandolfi, A. Gezerlis, and A. Schwenk, *Phys. Rev. Lett.* **113**, 192501 (2014).
- [45] M. Piarulli, A. Baroni, L. Girlanda, A. Kievsky, A. Lovato, E. Lusk, L. E. Marcucci, S. C. Pieper, R. Schiavilla, M. Viviani, and R. B. Wiringa, *Phys. Rev. Lett.* **120**, 052503 (2018).
- [46] M. Piarulli, L. Girlanda, R. Schiavilla, R. N. Pérez, J. E. Amaro, and E. R. Arriola, *Phys. Rev. C* **91**, 024003 (2015).
- [47] G. Baym and L. P. Kadanoff, *Phys. Rev.* **124**, 287 (1961).
- [48] A. D. Jackson, A. Lande, and R. A. Smith, *Phys. Rep.* **86**, 55 (1982).
- [49] A. D. Jackson and T. Wettig, *Phys. Rep.* **237**, 325 (1994).
- [50] R. Jastrow, *Phys. Rev.* **98**, 1479 (1955).
- [51] E. Feenberg, *Theory of Quantum Fluids* (Academic, New York, 1969).
- [52] C.-H. Yang and J. W. Clark, *Nucl. Phys. A* **174**, 49 (1971).
- [53] E. Krotscheck and J. W. Clark, *Nucl. Phys. A* **333**, 77 (1980).
- [54] S. Fantoni, *Nucl. Phys. A* **363**, 381 (1981).
- [55] A. Fabrocini, S. Fantoni, A. Y. Illarionov, and K. E. Schmidt, *Nucl. Phys. A* **803**, 137 (2008).
- [56] H.-H. Fan and E. Krotscheck, *Phys. Rep.* **823**, 1 (2019).
- [57] T. Morita, *Prog. Theor. Phys.* **20**, 920 (1958).
- [58] J. M. J. van Leeuwen, J. Groeneveld, and J. D. Boer, *Physica* **25**, 792 (1959).
- [59] A. D. Jackson, A. Lande, and R. A. Smith, *Phys. Rev. Lett.* **54**, 1469 (1985).
- [60] E. Krotscheck, R. A. Smith, and A. D. Jackson, *Phys. Rev. A* **33**, 3535 (1986).
- [61] S. Fantoni and S. Rosati, *Nuovo Cimento A* **43**, 413 (1978).
- [62] V. R. Pandharipande and R. B. Wiringa, *Rev. Mod. Phys.* **51**, 821 (1979).
- [63] E. Krotscheck, *Nucl. Phys. A* **482**, 617 (1988).
- [64] L. D. Landau, *Sov. Phys. JETP* **3**, 920 (1957).
- [65] L. D. Landau, *Sov. Phys. JETP* **5**, 101 (1957).
- [66] G. Baym and C. Pethick, *Landau Fermi Liquid Theory* (Wiley, New York, 1991).
- [67] C. H. Aldrich III and D. Pines, *J. Low Temp. Phys.* **32**, 689 (1978).
- [68] B. L. Friman and E. M. Nyman, *Nucl. Phys. A* **302**, 365 (1978).
- [69] W. Weise, *Nucl. Phys. A* **278**, 402 (1977).
- [70] J. W. Clark, in *Progress in Particle and Nuclear Physics*, edited by D. H. Wilkinson (Pergamon, Oxford, 1979), Vol. 2, pp. 89–199.
- [71] E. Krotscheck, *J. Low Temp. Phys.* **119**, 103 (2000).
- [72] E. Krotscheck, in *Introduction to Modern Methods of Quantum Many-Body Theory and their Applications*, Advances in Quantum Many-Body Theory, edited by A. Fabrocini, S. Fantoni, and E. Krotscheck (World Scientific, Singapore, 2002), Vol. 7, pp. 267–330.
- [73] R. A. Smith and A. D. Jackson, *Nucl. Phys. A* **476**, 448 (1988).
- [74] T. Kikuta, M. Morita, and M. Yamada, *Prog. Theor. Phys.* **15**, 222 (1956).
- [75] P. Hatzikonstantinou and J. M. Irvine, *J. Phys. A* **15**, 3627 (1982).
- [76] R. Balian and N. R. Werthamer, *Phys. Rev.* **131**, 1553 (1963).
- [77] R. Tamagaki, *Prog. Theor. Phys.* **44**, 905 (1970).
- [78] T. Takatsuka, *Prog. Theor. Phys.* **48**, 1517 (1972).
- [79] E. Krotscheck, R. A. Smith, and A. D. Jackson, *Phys. Rev. B* **24**, 6404 (1981).
- [80] M. Baldo, Ø. Elgarøy, L. Engvik, M. Hjorth-Jensen, and H.-J. Schulze, *Phys. Rev. C* **58**, 1921 (1998).
- [81] E. Krotscheck and J. W. Clark, *Nucl. Phys. A* **328**, 73 (1979).
- [82] E. Krotscheck and J. Springer, *J. Low Temp. Phys.* **132**, 281 (2003).
- [83] H.-H. Fan, E. Krotscheck, and J. W. Clark, *J. Low Temp. Phys.* **189**, 470 (2017).
- [84] H.-H. Fan, E. Krotscheck, T. Lichtenegger, D. Mateo, and R. E. Zillich, *Phys. Rev. A* **92**, 023640 (2015).
- [85] C. J. Pethick and H. Smith, *Bose-Einstein Condensation in Dilute Gases*, 2nd ed. (Cambridge University Press, Cambridge, 2008).
- [86] J. R. Schrieffer, *Theory of Superconductivity (Advanced Books Classics)*, revised ed. (Perseus Books, New York, 1999).
- [87] A. L. Fetter and J. D. Walecka, *Quantum Theory of Many-Particle Systems* (McGraw-Hill, New York, 1971).
- [88] X. R. Zhou, G. F. Burgio, U. Lombardo, H.-J. Schulze, and W. Zuo, *Phys. Rev. C* **69**, 018801 (2004).
- [89] J. M. Dong, U. Lombardo, and W. Zuo, *Phys. Rev. C* **87**, 062801(R) (2013).
- [90] K.-K. Voo, W. C. Wu, J.-X. Li, and T. K. Lee, *Phys. Rev. B* **61**, 9095 (2000).
- [91] S. T. Beliaev, in *Lecture Notes of the 1957 Les Houches Summer School*, edited by C. DeWitt and P. Nozières (Dunod, Malakoff, France, 1959), pp. 343–374.
- [92] R. W. Morse and H. V. Bohm, *Phys. Rev.* **108**, 1094 (1957).
- [93] E. Krotscheck, *Z. Phys.* **251**, 135 (1972).
- [94] See Supplemental Material at <http://link.aps.org/supplemental/10.1103/PhysRevC.109.015803> for a stand-alone code of our gap-equation solver together with a brief description on how it works.